Acta Pharmaceutica Sinica B 2022;12(6):2683–2694

Chinese Pharmaceutical Association
Institute of Materia Medica, Chinese Academy of Medical Sciences

Acta Pharmaceutica Sinica B

www.elsevier.com/locate/apsb
www.sciencedirect.com

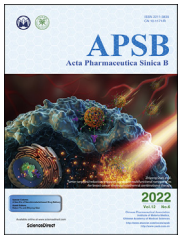

ORIGINAL ARTICLE

A hybrid bacterium with tumor-associated macrophage polarization for enhanced photothermal-immunotherapy

Jingya Zhao, Huabei Huang, Jinyan Zhao, Xiang Xiong, Sibo Zheng, Xiaoqing Wei, Shaobing Zhou*

Key Laboratory of Advanced Technologies of Materials, Ministry of Education, School of Materials Science and Engineering, Southwest Jiaotong University, Chengdu 610031, China

Received 8 August 2021; received in revised form 18 September 2021; accepted 15 October 2021

KEY WORDS

Immunotherapy;
Tumor-associated macrophage;
Immunogenic cell death;
Bifidobacterium;
Quantum dot

Abstract Remodeling the tumor microenvironment through reprogramming tumor-associated macrophages (TAMs) and increasing the immunogenicity of tumors *via* immunogenic cell death (ICD) have been emerging as promising anticancer immunotherapy strategies. However, the heterogeneous distribution of TAMs in tumor tissues and the heterogeneity of the tumor cells make the immune activation challenging. To overcome these dilemmas, a hybrid bacterium with tumor targeting and penetration, TAM polarization, and photothermal conversion capabilities is developed for improving antitumor immunotherapy *in vivo*. The hybrid bacteria (B.b@QDs) are prepared by loading Ag_2S quantum dots (QDs) on the *Bifidobacterium bifidum* (B.b) through electrostatic interactions. The hybrid bacteria with hypoxia targeting ability can effectively accumulate and penetrate the tumor tissues, enabling the B.b to fully contact with the TAMs and mediate their polarization toward M1 phenotype to reverse the immunosuppressive tumor microenvironment. It also enables to overcome the intratumoral heterogeneity and obtain abundant tumor-associated antigens by coupling tumor penetration of the B.b with photothermal effect of the QDs, resulting in an enhanced immune effect. This strategy that combines B.b-triggered TAM polarization and QD-induced ICD achieved a remarkable inhibition of tumor growth in orthotopic breast cancer.

Abbreviations: 4T1 cells, mouse mammary 4T1 tumor cells; $AgNO_3$, silver nitrate; B.b, *Bifidobacterium bifidum*; B.b@QDs, hybrid bacteria; CRT, calreticulin; CTLs, cytotoxic T lymphocytes; DLS, dynamic light scattering; EC cells, endothelial cells; GC, glycol chitosan; GSH, reduced glutathione; H&E, hematoxylin–eosin; ICD, immunogenic cell death; Na_2S, sodium sulfide; QDs, quantum dots; TAMs, tumor-associated macrophages; TEM, transmission electron microscopy; TUNEL, transferase-mediated UTP end labeling; XRD, X-ray diffraction.

*Corresponding author. Tel./fax: +86 28 87634076.
E-mail address: shaobingzhou@swjtu.edu.cn (Shaobing Zhou).

Peer review under responsibility of Chinese Pharmaceutical Association and Institute of Materia Medica, Chinese Academy of Medical Sciences.

https://doi.org/10.1016/j.apsb.2021.10.019

1. Introduction

At present, immunotherapy has attracted great attention in cancer therapy. It relies on activation of the immune system to attack the malignant tumor cells[1,2]. Current immunotherapy strategies mainly focus on activation of cytotoxic T lymphocytes (CTLs)[3,4]. However, the tumor microenvironment is immunosuppressive, which prevents the infiltration of the CTLs into tumors and weakens the immune response[5]. The immunosuppressive microenvironment is largely caused by the tumor-associated macrophages (TAMs), which constitute over 50% of the stromal cells within the tumors and are critical in tumor progression[6,7]. TAMs can be educated by the tumor cells and tend to exhibit the pro-tumor M2 phenotype to promote tumor invasion and metastasis[8−10]. The phenotype of the TAMs can also be reprogrammed from the pro-tumor M2 phenotype into anti-tumor M1 phenotype under some stimulations, which can produce the proinflammatory cytokines (IL-6, TNF-α, etc.) and activate the antitumor immune response[11−13]. The polarization of TAMs to M1 phenotype for cancer therapy has been achieved by using small molecule drugs or nanomedicines[14−16]. However, the low accumulation of small molecule drugs and poor penetration of nanomedicines in the tumor tissues often restrict their accessibility to TAMs due to their heterogeneous distribution in tumor microenvironment. Therefore, strategy that can target and penetrate the tumors and reprogram TAMs comprehensively for improving the antitumor immunotherapy efficacy is in great demand.

Many studies have shown that anaerobic bacteria can effectively target and penetrate the tumors[17,18]. The hypoxic environment in tumors provides an ideal habitat for anaerobic bacteria[19−22]. *Bifidobacterium* is a kind of anaerobic and probiotic bacteria, which has been widely used as a medicine for intestinal flora regulation[23]. Besides, *Bifidobacterium* also showed great potential in enhancing antitumor immunity[24,25]. They can migrate from the guts and colonize in the tumors[26]. Meanwhile, they can enhance the phagocytic activity of macrophages and induce an immune-favorable tumor microenvironment[26,27].

In addition to bacteria-mediated immune regulation, photothermal effect can also lead to a favorable tumor microenvironment for immune response[28]. Photothermal therapy not only can directly kill the tumor cells, but also can induce immunogenic cell death (ICD) of tumor cells, enabling the release of tumor associated antigens and the activation of dendritic cells to promote the recruitment of CTLs[29−31]. Moreover, photothermal therapy is a localized treatment method with high controllability and noninvasiveness[20,32−37]. Based on this, the combination of bacteria therapy and photothermal therapy might be a potential strategy to improve antitumor immunity. It may remodel the tumor microenvironment through reprogramming TAMs and increasing the immunogenicity of tumors for synergistic anticancer therapy.

Herein, a hybrid bacterium is developed to serve as an immunomodulator for polarizing M2 macrophages to M1 macrophages and inducing tumor ICD to achieve enhanced antitumor immune response. The hybrid bacteria were prepared by loading Ag_2S quantum dots (QDs) on the *Bifidobacterium bifidum* (B.b) through electrostatic interactions. As shown in Scheme 1, the hybrid bacteria with hypoxia targeting ability can effectively accumulate and penetrate the tumor tissues, enabling the B.b to fully contact with the TAMs and promote the polarization toward M1 phenotype to reverse the immunosuppressive tumor microenvironment. It also enables to overcome the intratumoral heterogeneity and obtain abundant tumor-associated antigens by coupling tumor penetration of the B.b with photothermal effect of the QDs, resulting in an enhanced immune effect. As a result, the upregulated secretion of proinflammatory cytokines and the activation of CTLs were detected, leading to a remarkable inhibition of tumor growth in orthotopic breast cancer.

2. Materials and methods

2.1. Chemicals and materials

Silver nitrate ($AgNO_3$), reduced glutathione (GSH) and sodium sulfide (Na_2S) were purchased from Aladdin Reagent (Shanghai) Co., Ltd. MRS liquid and agar media were purchased from Haibo Biological Technology Co., Ltd. Glycol chitosan (GC) was purchased from Sigma−Aldrich. ELISA kits for mouse TNF-α and IL-6 were purchased from eBioscience. All the antibodies for flow cytometry were purchased from Thermo Fisher Scientific. B.b was provided by the China Center of Industrial Culture Collection.

2.2. Cell lines and animals

Mouse mammary 4T1 tumor cells (4T1 cells), endothelial cells (EC cells) and macrophages cells (RAW264.7) were obtained from Sichuan University. They were cultured in DMEM medium (4T1 cells and RAW264.7) or F12 medium (EC cells) added with 10% fetal bovine serum. The peritoneal macrophages were collected from the mice. First, the BALB/c mice were intraperitoneally injected with starch broth (5%) for 3 days, and then fasted for 12 h. After this, they were sterilized with ethanol solution (75%) and DMEM medium was injected into the abdominal cavity. The suspension in the abdomen was aspirated and peritoneal macrophages were obtained. M2 macrophages were obtained by incubating the peritoneal macrophages with IL-4 (40 ng/mL) for 24 h.

BALB/c mice (female, aged 4−5 weeks) were fed in an experimental animal room at 37 °C with 55% of humidity. All animal experiments were performed in compliance with the guidelines approved by the Institutional Animal Care and Use Committee of Sichuan Academy of Medical Sciences.

2.3. Synthesis and characterization of the Ag_2S QDs

For the synthesis of the Ag_2S QDs, 400 μmol of GSH and 100 μmol of $AgNO_3$ were added to 75.0 mL of deionized water and stirred for a few minutes. Then, 25.0 mL of Na_2S solution was added under stirring. After this, the pH of the mixture was

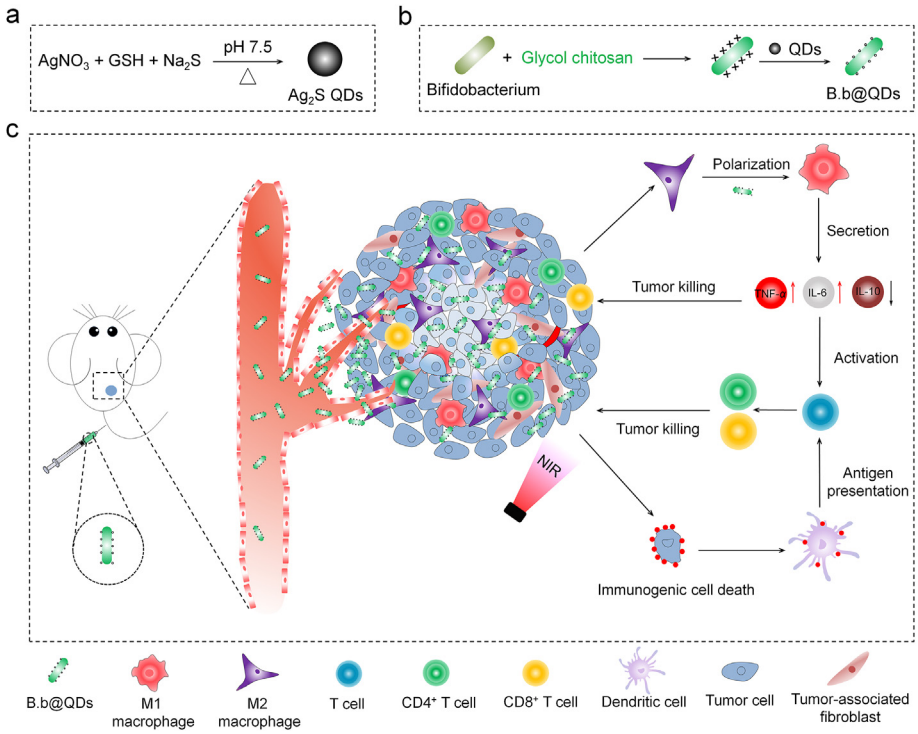

Scheme 1 (a) Schematic of the preparation of NIR Ag_2S QDs. (b) Schematic of the fabrication of the hybrid bacteria B.b@QDs. (c) Schematic of the hybrid bacteria combined with tumor targeting and penetration, tumor-associated macrophage polarization, and photothermal conversion capabilities for improving antitumor immunotherapy *in vivo*. The QD-hybrid bacteria with hypoxia targeting ability effectively accumulate and penetrate the tumor tissues, enabling them to fully contact with the tumor-associated macrophages and enhance the polarization of M2 macrophages to M1 macrophages. It also enables to overcome the intratumoral heterogeneity and obtain abundant tumor-associated antigens by coupling tumor penetration of the B.b with photothermal effect of the QDs.

adjusted to 7.5 with NaOH and heated at 95 °C for 3 h. The Ag_2S QDs were purified *via* centrifuge ultrafiltration (10 kDa MW).

Fluorescence spectrum was collected on a Lengguang F98 spectrophotometer. X-ray diffraction (XRD) data was obtained on a Philips X'Pert PRO XL-30 X-ray diffractometer. Transmission electron microscopy (TEM) and elemental mapping were performed on a Hitachi H-700H transmission electron microscope. Fourier transform infrared spectroscopy (FT-IR) were performed on a Thermo Nicolet 5700 instrument.

2.4. *Culture of B.b*

B.b (CGMCC 1.2212) was added to a sterilized centrifuge tube with a ratio of 10% bacterial solution and 90% MRS liquid culture medium. Then they were placed in an anaerobic incubator and cultured to reach the logarithmic growth phase. The bacteria were collected by centrifugation at 1000×*g* for 10 min at 4 °C and rinsed twice with sterile saline, and finally they were re-suspended with ice-cold sterile saline to adjust the bacteria concentration. Bacterial concentration was determined by plate colony-counting method.

2.5. *Preparation and characterization of the B.b@QDs*

To prepare the B.b@QDs, 100 μL of the bacteria (1×10^9 CFU/mL) was mixed with 100 μL of GC solution (1 mg/mL). After incubation for 30 min, the unbound GC was removed through centrifugation. Then 100 μL of Ag_2S QDs solution was added. After incubation for another 30 min, the B.b@QDs were obtained by centrifugation again.

The B.b@QDs dispersed in PBS buffer were dropped onto a carbon-coated copper net. Then TEM was used to observe the binding of QDs on the B.b. For fluorescence colocalization analysis, the FITC-labeled bacteria were modified with the QDs to obtain FITC and QD dual-labeled bacteria. The fluorescence imaging and flow cytometric analysis was performed to assess the labeling efficiency and the stability of the B.b with the QDs. The zetasizer instrument (Malvern) was used to detect the changes in zeta potential of the B.b before and after modification.

2.6. *Bacteria and cell activity assay*

In order to evaluate the activity of the bacteria after modification, B.b, B.b-GC and B.b@QDs containing equal amounts of B.b were diluted and cultured on solid MRS agar for 24 h to observe the growth of the bacteria. The numbers of bacterial colonies in each group were counted.

To evaluate the cytocompatibility of the QDs, the EC cells, RAW264.7 cells and 4T1 cells were incubated with different concentrations of QDs for 24 h. Then they were detected by alamar blue kit and calcein-AM/propidium iodide kit according to the instructions.

2.7. *Photothermal therapy in vitro*

To evaluate the photothermal effect, 1 mL of the QDs or B.b@QDs were irradiated under a near-infrared (NIR) laser (808 nm, 1.0 W/cm^2). During this process, the temperature was

measured with an infrared thermal imager. To detect the photothermal effect to tumor cells, 4T1 cells were treated with PBS + NIR, QDs, QDs + NIR, B.b, B.b@QDs or B.b@QDs + NIR and then the cell viability was measured by live/dead cell fluorescence staining.

2.8. ICD in vitro

To evaluate the ICD of tumor cells induced by the B.b@QDs + NIR, the exposure of calreticulin (CRT) on tumor cell membrane were detected. 24 h after treated with QDs + NIR or B.b@QDs + NIR, the 4T1 cells were fixed and incubated with CRT monoclonal antibody under shaking. Then the FITC-labeled secondary antibody was added and incubated. After staining with DAPI, the cells were observed on a confocal microscope (Zeiss) and detected by flow cytometry.

2.9. Macrophage polarization with the B.b@QDs

Mouse peritoneal macrophages were used to verify the polarization effects of different formulations. After polarized to M2 phenotype by IL-4, the peritoneal macrophages were incubated with the materials for 3 h. After this, the excess materials were removed by washing and the macrophages were cultured for 24 h. Then, the macrophages were washed and incubated with antibodies (FITC-anti-CD80, FITC-anti-CD206, APC-anti-F4/80) at 4 °C for 30 min. Next, the macrophages were filtered through a 200 mesh membrane and detected by flow cytometry. Beckman CytoFLEX flow cytometry was used to detect the signals and the data was analyzed using Flowjo software.

To measure the cytokines secreted by macrophages after polarization, M2 macrophages were cultured in the 6-well plates (5×10^5/well) and incubated with different materials for 24 h. Subsequently, the cell supernatant was collected for cytokine assay. Briefly, the release of TNF-α and IL-6 was detected by ELISA according to the protocols. The concentration of the cytokines can be obtained through a pre-built calibration curve on the basis of the UV−Vis absorption of the samples.

2.10. Immunotherapy in vitro

The immunotherapy *in vitro* was assessed with a transwell system. First, M2 macrophages and 4T1 cells were cultured in the upper chambers and lower chambers of the transwell system with a ratio of 1:4 for 24 h, respectively. Then, QDs, B.b or B.b@QDs were added to the upper chambers and incubated for 24 h. The viability of the 4T1 tumor cells was detected by alamar blue assay.

2.11. Biodistribution and tumor penetration of the B.b@QDs in vivo

To establish the tumor model, each 4−5 weeks old female BALB/c mouse was injected with 2×10^6 4T1 cells on the mammary glands. When reaching about 50 mm^3 in tumor volume, the treatment experiments began.

To evaluate the biodistribution *in vivo*, NIR fluorescence imaging was performed after intravenous administration of QDs or B.b@QDs. The NIR fluorescence imaging of the mice were performed at 1, 4, 12, 24 and 48 h post-injection. The mice were euthanized, and the tumor and main organs were harvested and imaged at 24 h post-injection. The tumor tissues were also sectioned for Gram staining analysis.

To evaluate tumor penetration of the bacteria, 4T1 tumor-bearing mice were intravenously injected with QDs or B.b@QDs. At 24 h post-injection, the mice were sacrificed, and the tumor tissues were harvested and prepared into frozen sections. After staining with DAPI, the slices were observed with a fluorescence microscope (Zeiss).

2.12. Anti-tumor immunity activation of the B.b@QDs in vivo

For photothermal imaging, the 4T1 tumor-bearing mice were injected with PBS, QDs, B.b or B.b@QDs. After 24 h, the mice were anesthetized and irradiated with an 808 nm laser (1.5 W/cm^2). During this process, infrared thermal images of the mice were collected and analyzed (SmartView software).

Two days after photothermal therapy, ICD of the tumor tissues were evaluated by Western blot analysis. After lysed by RIPA lysis, the CRT proteins in the tumor tissues were separated by SDS-PAGE, transferred to a PVDF membrane and detected with electrochemiluminescence immunoassay.

To verify the polarization of the macrophages by the B.b@QDs in the tumor microenvironment, the phenotype of the macrophages was detected by flow cytometry on Day 3. The tumor tissue was collected, washed, cut into smaller pieces, and then homogenized to obtain a tissue homogenate. The tumor cell suspension was filtered through a 200-mesh membrane. After that, 500 μL of erythrocyte lysate was added and then cell suspension was centrifuged at 350×*g* for 5 min to remove the lysates. Then the cells were washed and re-suspended with PBS. Next, the cells were stained with F4/80, CD80 and CD206 antibodies at 4 °C for 30 min and detected by flow cytometry.

To detect the cytokines secreted by macrophages in the tumor tissues, immunohistochemical staining of IL-6, TNF-α and IL-10 after the treatment was carried out on Day 14. Immunohistochemical staining of IL-6, TNF-α and IL-10 was performed on the tumor sections according to the instructions of the immunohistochemistry kit. Finally, the cytokines expressed on the tumor cells were observed through an optical microscope.

To evaluate T lymphocyte activity in the tumor microenvironment, immunohistochemical staining of $CD8^+$ and $CD4^+$ T cells was performed on Day 14. The tumor tissue sections were incubated with $CD8^+$ and $CD4^+$ antibodies and FITC-labeled secondary antibodies. After this, fluorescence images of $CD8^+$ and $CD4^+$ T cells were performed by using a fluorescence microscope (Zeiss).

2.13. In vivo anti-tumor study

When the tumor reached about 50 mm^3, the mice were randomly divided into six groups ($n = 5$) and the treatment experiment began. PBS + NIR, QDs, QDs + NIR, B.b + NIR, B.b@QDs or B.b@QDs + NIR were injected into the mice through the tail vein on days 0, 3, 6. The tumor volume and mouse body weight were measured every three days.

2.14. Routine blood test

After the treatments ended on Day 21, the blood of the mice was sampled. Then a standard blood analyzer was used for routine blood test.

3. Results and discussion

3.1. Preparation and characterization of the hybrid bacteria

Ag_2S QDs have been found to possess NIR fluorescence emission and NIR photothermal effect, making them promising in biological imaging and tumor therapy[38,39]. In this work, the Ag_2S QDs were used to monitor the biodistribution of the hybrid bacteria and induce ICD of the tumor cells. The Ag_2S QDs were synthesized by a hydrothermal method according to the literature with some modifications[40] (Scheme 1a). Briefly, $AgNO_3$, GSH and water were mixed to enable the binding of Ag^+ with GSH. Then Na_2S was added to trigger the nucleation of the QDs. The mixture was heated at 95 °C for 3 h for further growth of the QDs. The TEM image (Fig. 1a) revealed that the Ag_2S QDs were uniform spherical nanoparticles, with an average size of 5.3 nm. The XRD pattern of the QDs showed broad and overlapped diffraction peaks, probably due to their small size (Supporting Information Fig. S1a). The FT-IR spectrum (Supporting Information, Fig. S1b) revealed that the GSH might bind on the QDs through Ag-S bond since no noticeable absorption peak corresponding to free thiol group (2490 cm^{-1}) was detected in the QDs. The fluorescence emission peak of the Ag_2S QDs was at 816 nm (Fig. S1c). Within continuous irradiation of half an hour, the fluorescence intensity of the QDs decreased only by 14.7% (Supporting Information Fig. S2), indicating that they had good fluorescence stability. Besides NIR fluorescence, they also showed NIR photothermal effect under 808 nm laser irradiation. During the five irradiation/cooling cycles, the Ag_2S QDs showed stable photothermal effect and the photothermal conversion efficiency was 29.2% (Supporting Information Fig. S3).

The hybrid bacteria (B.b@QDs) were prepared by loading Ag_2S QDs on the B.b through electrostatic interactions according to a previous report with some modifications[41]. The assembly of the negatively charged QDs on the bacteria was mediated by GC (Scheme 1b). First, GC with positive charge was coated on the B.b. Then the QDs bound with the bacteria *via* electrostatic absorptions. Representative TEM images of the B.b (Supporting Information, Fig. S4a) and B.b@QDs (Fig. 1b and Fig. S4b) were displayed. After modification with the QDs, there was no significant change in the morphology of the bacteria and they remained forked. As can be seen in Fig. 1b and c, some nanoparticles were on the bacteria in the B.b@QDs group. The high resolution TEM image revealed that the lattice fringes of the nanoparticles on the bacteria are the (122) planes of Ag_2S (Fig. 1c), indicating successful binding of the QDs on the bacteria. The EDX element mapping showed the presence of both silver and sulfur elements on the bacteria (Fig. 1d), also suggesting the successful preparation of the hybrid bacteria.

Then, FITC-labeled bacteria were loaded with the QDs and observed *via* fluorescence microscopy after 3 times of washing. As shown in Fig. 1e, almost all the NIR fluorescence signals of the QDs colocalized with the green fluorescence signals of FITC, demonstrating the highly efficient modification of the bacteria with the QDs. The assembly of the negatively charged QDs on the bacteria was mediated by GC and the resulting B.b@QDs still charged negatively (Supporting Information Fig. S5a). This assembly was very controllable and the content of the QDs on the bacteria could be controlled by adjusting the GC concentration (Fig. S5b). The GC concentration of 1 mg/mL was chosen for the subsequent preparation of the B.b@QDs based on the optimization. At this condition, the positive percentage of the QDs modified B.b reached as high as 95.7%, quantitatively evaluated by flow cytometry (Fig. 1f). To evaluate the stability of the QDs on the bacteria, the hybrid bacteria were incubated with a culture medium for 48 h under shaking at 37 °C and then measured by

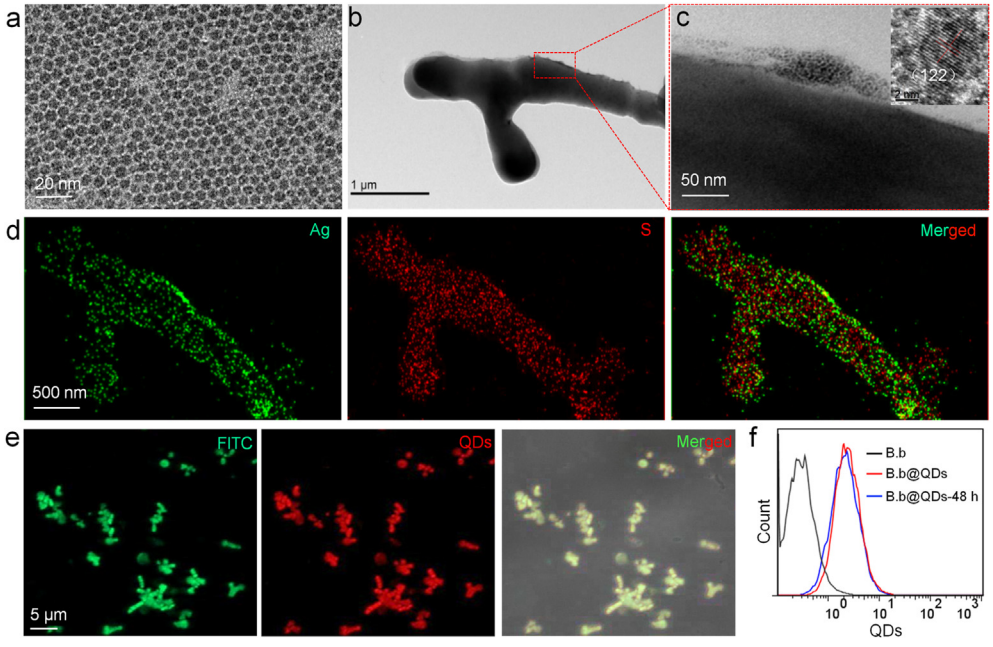

Figure 1 Characterization of the hybrid bacteria. (a) TEM image of the Ag_2S QDs. (b) TEM image of the B.b@QDs, (c) High resolution TEM image of the B.b@QDs and the Ag_2S QDs on the B.b@QDs (inset). (d) Elemental mapping images of the Ag_2S QDs on the B.b@QDs. (e) Fluorescence images of FITC-labeled B.b after modified with the Ag_2S QDs. (f) Flow cytometric histograms of the B.b, B.b@QDs and B.b@QDs-48 h (incubation with DMEM medium for 48 h).

flow cytometry. As shown in Fig. 1f and Supporting Information Fig. S6, no significant decrease in QD signals was detected, suggesting good stability of the QDs on the bacteria.

3.2. *Photothermal therapy and ICD in vitro*

After the QD modification, the viability of the B.b was not significantly affected and the survival rate retained approximately 75% (Supporting Information Fig. S7). The hybrid bacteria inherited the NIR photothermal effect from the QDs and the photothermal conversion efficiency of the B.b@QDs was 29.9% (Supporting Information Fig. S8). Under the irradiation of 808 nm laser for 10 min, the temperature of the QDs and the B.b@QDs solution raised about 10 °C (Fig. 2a and b). While the hybrid bacteria had the photothermal conversion ability, their activity was expected not to be affected. So the temperature tolerance of the bacteria was then examined. It was found that they can still maintain high activity at 45 °C (Supporting Information Fig. S9), which can also meet the demand of photothermal treatment of tumors. To confirm this, the viability of 4T1 tumor cells were evaluated *via* live/dead cell staining assay after being pretreated with the hybrid bacteria under the laser irradiation. During the irradiation, the temperature was carefully controlled to maintain at 45 °C for 10 min in both the QDs + NIR group and the B.b@QDs + NIR group. In these two groups, almost all the cells died in the irradiation area while no dead cells were observed in other groups without NIR photothermal effect (Fig. 2c and Supporting Information Fig. S10).

The photothermal effect of the hybrid bacteria is further expected to induce ICD of the tumor cells[42]. The exposure of CRT on tumor cell membrane, a sign of ICD, was detected by immunofluorescence staining. As shown in Fig. 2d, there were CRT fluorescence signals on 4T1 tumor cells in the QDs + NIR group and B.b@QDs + NIR group, suggesting the photothermal treatment led to ICD. The flow cytometry was performed to further detect the CRT quantitatively. The positive rate of CRT in the B.b@QDs + NIR group was 34.3%, slightly higher than that in the QDs + NIR group (32.9%, Fig. 2e). All the results indicated that the hybrid bacteria with photothermal effect could trigger ICD of the tumor cells.

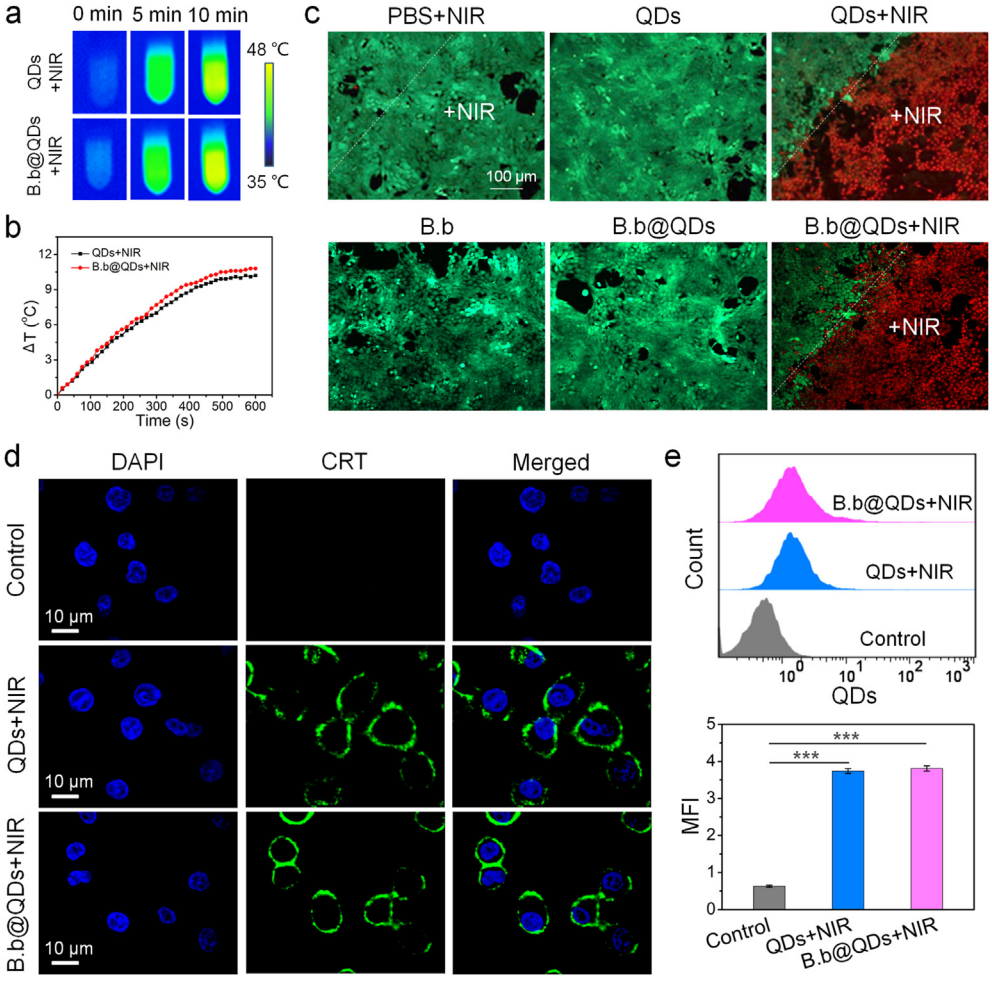

Figure 2 *In vitro* photothermal therapy and ICD induced by the hybrid bacteria. (a) Infrared thermal images of the QDs and B.b@QDs under the irradiation of 808 nm laser (1.0 W/cm^2). (b) Temperature curves of the QDs and B.b@QDs under NIR laser irradiation. (c) Fluorescence images showing the cell viability of 4T1 cells treated with different materials. (d) Fluorescence images of CRT expressed on the 4T1 tumor cells after treated by different materials. (e) Flow cytometric histograms and corresponding mean fluorescence intensity of CRT expressed on 4T1 tumor cells after different treatment ($n = 3$). ***$P < 0.001$.

3.3. *Polarization of macrophages by the hybrid bacteria in vitro*

In order to verify the immune activation ability of the B.b, the polarization of the peritoneal macrophages from M2 to M1 phenotype with the hybrid bacteria was tested *in vitro*. The flow cytometric analysis showed that the expression of CD80 (a sign of M1 macrophage) in the B.b group and the B.b@QDs group increased to 78.21% and 71.78%, respectively (Fig. 3a). Meanwhile, the expression of CD206, a sign of M2 macrophage, in the above two groups decreased to 25.1% and 29.3%, respectively. However, the QDs group exhibited no significant polarization effect since the expression of CD80 was only 8.65%. The activation of the macrophages by the hybrid bacteria might be mediated by the recognition and phagocytosis of the bacteria with the macrophages. As illustrated in Supporting Information Fig. S11, the engulfing of the B.b@QDs by the macrophages was observed on a fluorescence microscope.

After the reprograming, we tested the changes of the immune promoting cytokines secreted by M1 macrophages using the ELLISA kit. The results showed that the expression level of the TNF-α and IL-6 was significantly increased under the action of the B.b and the B.b@QDs (Fig. 3b). The contents of the TNF-α and IL-6 in the B.b@QDs group were 3.7 and 2.9 times higher than those in the control group, respectively. It was reported that TNF-α could directly induced apoptosis of the tumor cells[43]. To further investigate the polarization of macrophages enhanced the killing effect to 4T1 cells, a transwell system was fabricated, as depicted in Fig. 3c. The survival rate of the 4T1 cells in the B.b group and the B.b@QDs group decreased to 42.7% and 48.0%, respectively (Fig. 3d). However, without the B.b, no significant killing effect was observed and the survival rate retained 96.8% in the QDs group. The above results showed that the hybrid bacteria could polarize the macrophages into tumoricidal M1 phenotype and thus enhance the killing ability to cancer cells.

3.4. *Biodistribution and tumor penetration of the hybrid bacteria in vivo*

The tumor targeting of the hybrid bacteria *in vivo* was monitored *via* NIR fluorescence imaging after the intravenous injection. In the

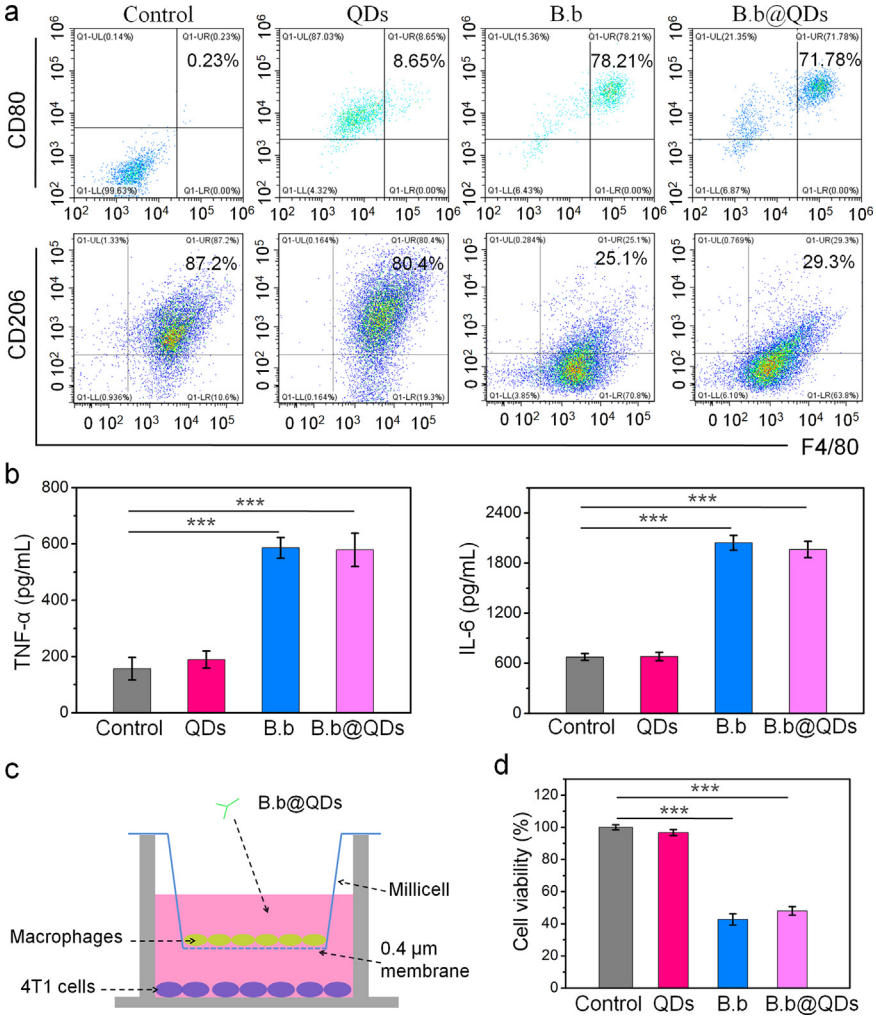

Figure 3 Polarization of macrophages by the hybrid bacteria *in vitro*. (a) Surface markers of M1 macrophages ($CD80^+$, $F4/80^+$) and M2 macrophages ($CD206^+$, $F4/80^+$) in different groups, detected by flow cytometry. (b) Concentration of TNF-α and IL-6 in the supernatant after co-incubation of macrophages with different materials ($n = 3$). The cytokine expression level was detected by ELISA. (c) Schematic illustration of a transwell system, which is used to detect immune response *in vitro*. (d) Cell viability of 4T1 cells in the transwell system after treated with different materials ($n = 3$). ***$P < 0.001$.

B.b@QDs group, strong NIR fluorescence at the tumor site was observed at 24 h after the injection and the signal could still be observed at 48 h post-injection (Fig. 4a). However, in free QDs group, no significant accumulation in the tumor was observed during the 48 h. Moreover, the tumor and main organs were harvest and imaged to directly evaluate the bio-distribution at 24 h post-injection. As shown in Supporting Information Fig. S12, the ICP-MS results were consistent with the *in vivo* imaging results, which showed a significant accumulation of the B.b@QDs in the tumor. This might be attributed to the hypoxia-specific targeting of tumor mediated by the bacteria. The free QDs exhibited no significant accumulation in both the tumor and the organs, probably due to the rapid elimination of the small sized QDs from the body. In addition, Gram staining of the tumor sections from the B.b@QDs group was performed to observe the bacteria. The results showed that B.b existed in the tumor tissues, as indicated by the arrows in Fig. 4b.

Based on this, we further evaluated whether the hybrid bacteria could penetrate the tumor and reach the hypoxic tumor cores. The fluorescence images of the tumor sections showed that the B.b@QDs distributed throughout the whole tumor about 1 cm in diameter, suggesting that they could penetrate the tumor deeply (Fig. 4c). Compared with the bacteria group, the free QDs group showed very weak fluorescence signals due to their low accumulation in the tumors. These results demonstrated that the hybrid bacteria could specifically target and deeply penetrate the tumor tissues.

3.5. *Antitumor immunity activation of the hybrid bacteria in vivo*

We further investigated whether the hybrid bacteria combined with tumor targeting and penetration, macrophage polarization and photothermal conversion capabilities could activate antitumor immunity *in vivo*. The NIR photothermal treatment of the mice bearing 4T1 breast tumor was carried out at 24 h post-injection, and the temperature was monitored *via* photothermal imaging. Under the irradiation of 808 nm laser for 10 min, the temperature at the tumor site in the B.b@QDs + NIR group reached 45 °C while other groups had only a little or no rise in temperature (Fig. 5a and b). The temperature was maintained for another 10 min for photothermal treatment. Two days after the photothermal treatment, the CRT expressed by tumor cells was tested through Western blot analysis. The results showed that the B.b@QDs + NIR group had a higher expression level of CRT compared to the QDs + NIR group (Fig. 5c), which might be due to more accumulation of the B.b@QDs in tumor. These results indicated that the hybrid bacteria combined with NIR laser irradiation can induce ICD to the tumor cells *in vivo*.

In addition, the phenotype of the macrophages in the tumor tissues was detected by flow cytometry. The relative number of M1 macrophages ($CD80^+$, $F4/80^+$) in the B.b@QDs + NIR group increased from 10.01% to 19.78% and the relative

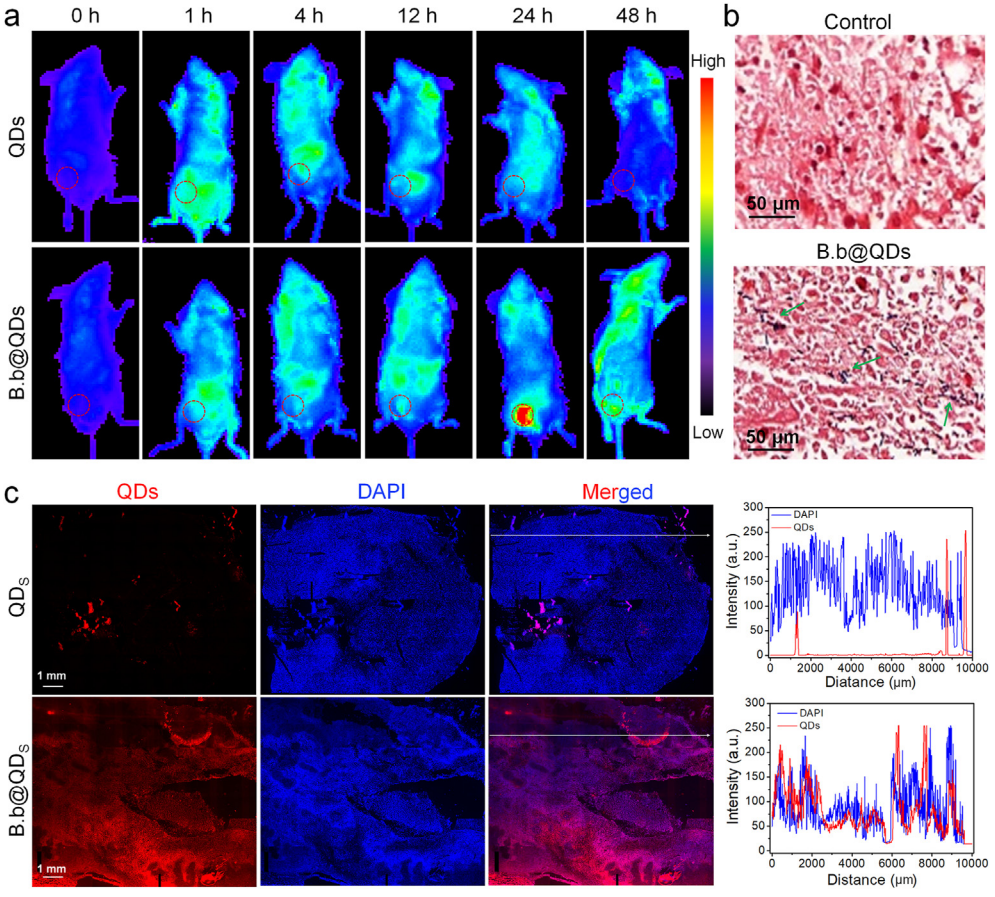

Figure 4 Biodistribution and tumor penetration of the hybrid bacteria *in vivo*. (a) NIR fluorescence images showing the biodistribution of free QDs or B.b@QDs in the body of mice. (b) Gram staining images of tumor tissue sections from the PBS group and the B.b@QDs group. The green arrows point to the bacteria. (c) Fluorescence images of the 4T1 tumors with the maximum sections at 24 h after the injection of QDs or B.b@QDs and corresponding line profiles.

number of M2 macrophages ($CD206^+$, $F4/80^+$) decreased from 40.59% to 26.8% compared with the control group (Fig. 5d). The deep penetration of the hybrid bacteria in the tumor made them fully contact with the TAMs and led to a good polarization effect, and the M1/M2 ratio in the B.b@QDs + NIR group (0.74) was 1.7-fold that in the QDs + NIR group (0.43, Supporting Information Fig. S13). Moreover, we found that the M1/M2 ratio in the B.b@QDs + NIR group (0.74) was also higher than those in the B.b + NIR group (0.53) and the B.b@QDs group (0.58). Since the QDs had no significant

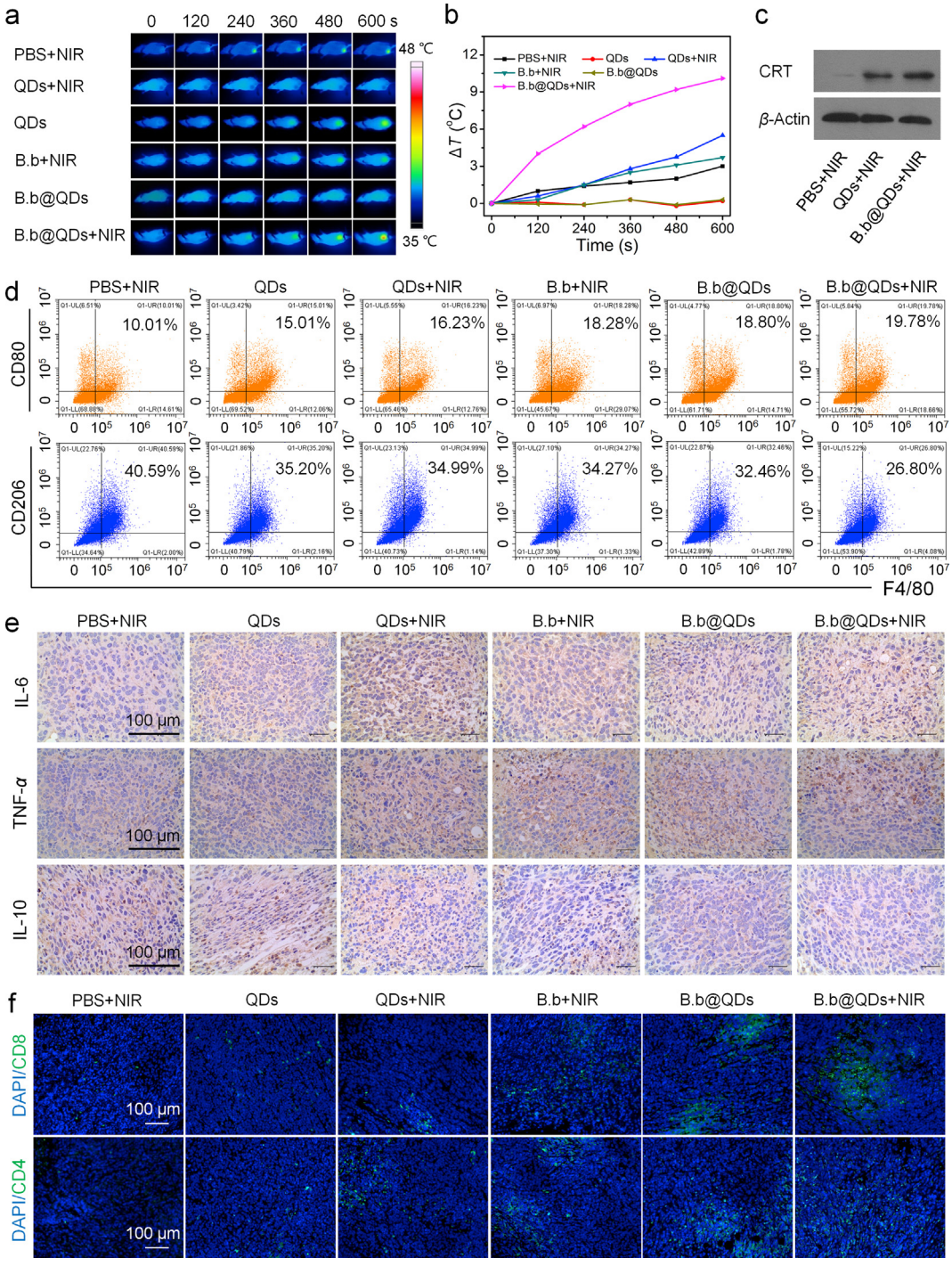

Figure 5 Antitumor immunity activation of the hybrid bacteria *in vivo*. Infrared thermal images (a) of 4T1 tumor-bearing mice intravenously injected with various formulations with or without 808 nm NIR laser irradiation and the corresponding heating curves (b) at the tumor sites in mice. (c) Expression of CRT in tumor tissues of the BALB/c mice after treated with different formulations. (d) Surface markers of M1 macrophages ($CD80^+$, $F4/80^+$) and M2 macrophages ($CD206^+$, $F4/80^+$) from the tumor tissues of the BALB/c mice after treated with different formulations, detected by flow cytometry. (e) Immunohistochemical staining images of IL-6, TNF-α, IL-10 in the tumor tissues from different groups. (f) Immunofluorescence images of the $CD8^+$ and $CD4^+$ T cells in the tumor tissues from different groups.

polarization effect, this might be ascribed to the photothermal effect-enhanced tumor polarization[44]. The polarization of the TAM from M2 to M1 phenotype by the hybrid bacteria led to a significant up-regulating of the pro-inflammatory cytokines, such as TNF-α and IL-6, and a significant down-regulating of the immunosuppressive cytokines, such as IL-10 (Fig. 5e). The immunogenic cell death and the macrophage polarization could enhance T lymphocyte activity and the $CD8^+$ and $CD4^+$ T cells in the tumor tissues were detected *via* immunofluorescence staining. As shown in Fig. 5f, no significant fluorescence signals from the $CD8^+$ and $CD4^+$ T cells were observed in the free QDs group and the QDs+NIR group, probably due to their low accumulation in the tumors and weak immunity activation. There were a number of $CD8^+$ and $CD4^+$ T cells in the B.b+NIR group, the B.b@QDs group and the B.b@QDs + NIR group, possibly because the polarization of the macrophages by them stimulated the T lymphocyte response. Taken together, the polarization of the macrophages and the ICD of the tumors induced by the hybrid bacteria collaboratively enhanced the anti-tumor immune activation of T cells.

3.6. *Antitumor efficacy of the hybrid bacteria in vivo*

The hybrid bacteria could active antitumor immune response in the tumor microenvironment, and the antitumor effect *in vivo* was further investigated. As shown in Fig. 6a–c, the QDs group showed no obvious tumor inhibition compared with the PBS group, perhaps because of their low accumulation in the tumors. By using the bacteria as carriers, the tumor accumulation and penetration were enhanced and the macrophage polarization was promoted. The inhibition rates of the B.b + NIR group and the B.b@QDs group were 58.8% and 57.3%, respectively (Fig. 6d). The B.b@QDs + NIR group with both macrophage polarization and photothermal therapy capabilities showed the best anti-tumor effect and the tumor inhibition rate was 77.3%. The mouse weight was recorded every 3 days after the first injection. During the 21 days of the treatment, there was no obvious weight loss in all the groups (Fig. 6e), indicating no systematic toxicity of the treatment.

The antitumor effect of the hybrid bacteria was further investigated by H&E and TUNEL staining analyses. The H&E staining results indicated that the tumor tissues treated by the bacteria, especially by the B.b@QDs + NIR, exhibited a remarkable nuclear condensation and fragmentation (Fig. 6f). Whereas, in other groups, the tumor cells remained the normal morphologies. The results from TUNEL staining also indicated that the B.b@QDs + NIR group had a relatively higher level of cell apoptosis. Overall, the hybrid bacteria targeted and penetrated the tumor tissues, polarized the TAM, induced ICD of the tumor cells and finally led to a good antitumor immunotherapy effect.

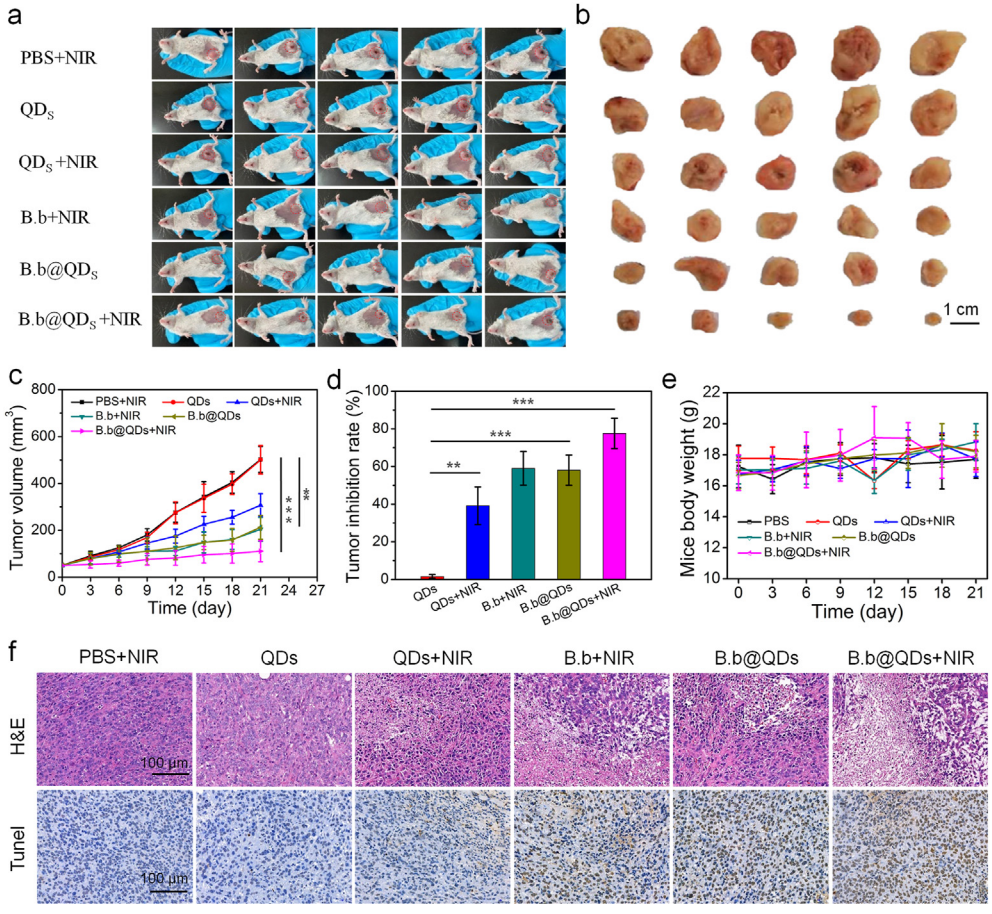

Figure 6 *In vivo* antitumor effect. Photos of the mice (a) and the excised tumors (b) at the end of treatment on Day 21. Changes of tumor volume (c), tumor inhibition rate (d) and body weight (e) of the mice receiving different treatments ($n = 5$). (f) H&E and TUNEL staining images of the tumor tissues from the mice at the end of the treatment. $^{**}P < 0.01$, $^{***}P < 0.001$.

3.7. *Biosafety of the hybrid bacteria in vivo*

The biosafety of the bacteria *in vivo* was evaluated by hematologic analysis after the treatment ended on Day 21. The blood routine indexes in the hybrid bacteria group were almost consistent with those in the PBS group, suggesting good biocompatibility of the hybrid bacteria (Supporting Information Fig. S14). Nonetheless, the long term toxicity still needs to be evaluated before their clinical transformation.

4. Conclusions

In summary, we have developed a hybrid bacterium that can polarize M2 macrophages to M1 macrophages and induce ICD of tumor cells for improving antitumor immune response *in vivo*. Due to the hypoxia targeting of B.b, the hybrid bacteria showed remarkable accumulation in tumor and could penetrate the whole tumor up to 1 cm in diameter. With the polarization of the hybrid bacteria, the ratio of M1/M2 in tumor tissues increased by 1.3 times, promoting the secretion of proinflammatory cytokines and the activation of antitumor immunity. They also induced ICD under the photothermal effect of QDs and improved the infiltration of CTLs in the tumor tissues, further enhancing the immune effect and inhibiting the tumor growth. More importantly, the hybrid bacteria, which used the intestinal probiotics as the immunomodulator and carrier, had good biocompatibility *in vivo*, enabling their clinical transformation.

Acknowledgments

This study was supported by the National Natural Science Foundation of China (51725303, 81701831, 52033007), the Sichuan Science and Technology Program (2020YFH0046, China) and the Fundamental Research Funds for the Central Universities (2682021CG017, China). The authors thank Analytical and Testing Center of Southwest Jiaotong University.

Author contributions

Jingya Zhao and Shaobing Zhou designed the research. Jingya Zhao and Huabei Huang carried out the experiments and performed data analysis. Jinyan Zhao, Xiang Xiong, Sibo Zheng and Xiaoqing Wei participated part of the experiments. Jingya Zhao and Huabei Huang wrote the manuscript. Shaobing Zhou revised the manuscript. All of the authors have read and approved the final manuscript.

Conflicts of interest

The authors declare no conflicts of interest.

Appendix A. Supporting information

Supporting information to this article can be found online at https://doi.org/10.1016/j.apsb.2021.10.019.

References

1. Khalil DN, Smith EL, Brentjens RJ, Wolchok JD. The future of cancer treatment: immunomodulation, CARs and combination immunotherapy. *Nat Rev Clin Oncol* 2016;**13**:273–90.
2. Nam J, Son S, Park KS, Zou WP, Shea LD, Moon JJ. Cancer nanomedicine for combination cancer immunotherapy. *Nat Rev Mater* 2019;**4**:398–414.
3. O'Donnell JS, Teng MWL, Smyth MJ. Cancer immunoediting and resistance to T cell-based immunotherapy. *Nat Rev Clin Oncol* 2019;**16**:151–67.
4. Farhood B, Najafi M, Mortezaee K. $CD8^+$ cytotoxic T lymphocytes in cancer immunotherapy: a review. *J Cell Physiol* 2019;**234**:8509–21.
5. Munn DH, Bronte V. Immune suppressive mechanisms in the tumor microenvironment. *Curr Opin Immunol* 2016;**39**:1–6.
6. Zhou JW, Tang ZW, Gao SY, Li CY, Feng YT, Zhou XK. Tumor-associated macrophages: recent insights and therapies. *Front Oncol* 2020;**10**:188.
7. Lei X, Lei Y, Li JK, Du WX, Li RG, Yang J, et al. Immune cells within the tumor microenvironment: biological functions and roles in cancer immunotherapy. *Cancer Lett* 2020;**470**:126–33.
8. Liu Y, Cao XT. The origin and function of tumor-associated macrophages. *Cell Mol Immunol* 2015;**12**:1–4.
9. Chen YB, Song YC, Du W, Gong LL, Chang HC, Zou ZZ. Tumor-associated macrophages: an accomplice in solid tumor progression. *J Biomed Sci* 2019;**26**:78.
10. Lin YX, Xu JX, Lan HY. Tumor-associated macrophages in tumor metastasis: biological roles and clinical therapeutic applications. *J Hematol Oncol* 2019;**12**:76.
11. Anfray C, Ummarino A, Andon FT, Allavena P. Current strategies to target tumor-associated-macrophages to improve anti-tumor immune responses. *Cells* 2020;**9**:46.
12. Mantovani A, Marchesi F, Malesci A, Laghi L, Allavena P. Tumour-associated macrophages as treatment targets in oncology. *Nat Rev Clin Oncol* 2017;**14**:399–416.
13. Wei B, Pan J, Yuan R, Shao B, Wang Y, Guo X, et al. Polarization of tumor-associated macrophages by nanoparticle-loaded *Escherichia coli* combined with immunogenic cell death for cancer immunotherapy. *Nano Lett* 2021;**21**:4231–40.
14. Liu L, Wang Y, Guo X, Zhao J, Zhou S. A biomimetic polymer magnetic nanocarrier polarizing tumor-associated macrophages for potentiating immunotherapy. *Small* 2020;**16**:2003543.
15. Rodell CB, Arlauckas SP, Cuccarese MF, Garris CS, Ahmed RLMS, Kohler RH, et al. TLR7/8-agonist-loaded nanoparticles promote the polarization of tumour-associated macrophages to enhance cancer immunotherapy. *Nat Biomed Eng* 2018;**2**:578–88.
16. Li DD, Zhang M, Xu F, Chen YZ, Chen BF, Chang Y, et al. Biomimetic albumin-modified gold nanorods for photothermo-chemotherapy and macrophage polarization modulation. *Acta Pharm Sin B* 2018;**8**:74–84.
17. Yi C, Huang Y, Guo ZY, Wang SR. Antitumor effect of cytosine deaminase/5-fluorocytosine suicide gene therapy system mediated by *Bifidobacterium infantis* on melanoma. *Acta Pharmacol Sin* 2005;**26**:629–34.
18. Luo CH, Huang CT, Su CH, Yeh CS. Bacteria-mediated hypoxia-specific delivery of nanoparticles for tumors imaging and therapy. *Nano Lett* 2016;**16**:3493–9.
19. Chen WF, Wang Y, Qin M, Zhang XD, Zhang ZR, Sun X, et al. Bacteria-driven hypoxia targeting for combined biotherapy and photothermal therapy. *ACS Nano* 2018;**12**:5995–6005.
20. Chen FM, Zang ZS, Chen Z, Cui L, Chang ZG, Ma AQ, et al. Nanophotosensitizer-engineered Salmonella bacteria with hypoxia targeting and photothermal-assisted mutual bioaccumulation for solid tumor therapy. *Biomaterials* 2019;**214**:119226.
21. Fang J, Islam W, Maeda H. Exploiting the dynamics of the EPR effect and strategies to improve the therapeutic effects of nanomedicines by using EPR effect enhancers. *Adv Drug Deli Rev* 2020;**157**:142–60.

22. Felfoul O, Mohammadi M, Taherkhani S, Lanauze DD, Xu YZ, Loghin D, et al. Magneto-aerotactic bacteria deliver drug-containing nanoliposomes to tumour hypoxic regions. *Nat Nanotechnol* 2016;**11**:941−7.
23. Arboleya S, Watkins C, Stanton C, Ross RP. Gut bifidobacteria populations in human health and aging. *Front Microbiol* 2016;**7**:1204.
24. Wang F, Yin Q, Chen L, Davis MM. *Bifidobacterium* can mitigate intestinal immunopathology in the context of CTLA-4 blockade. *Proc Natl Acad Sci U S A* 2018;**115**:157−61.
25. Matson V, Fessler J, Bao R, Chongsuwat T, Zha YY, Alegre ML, et al. The commensal microbiome is associated with anti-PD-1 efficacy in metastatic melanoma patients. *Science* 2018;**359**:104−8.
26. Shi YY, Zheng WX, Yang KT, Harris KG, Ni KY, Xue L, et al. Intratumoral accumulation of gut microbiota facilitates CD47-based immunotherapy *via* STING signaling. *J Exp Med* 2020;**217**:20192282.
27. Sivan A, Corrales L, Hubert N, Williams JB, Aquino-Michaels K, Earley ZM, et al. Commensal *Bifidobacterium* promotes antitumor immunity and facilitates anti-PD-L1 efficacy. *Science* 2015;**350**:1084−9.
28. Huang LP, Li YN, Du YN, Zhang YY, Wang XX, Y, et al. Mild photothermal therapy potentiates anti-PD-L1 treatment for immunologically cold tumors *via* an all-in-one and all-in-control strategy. *Nat Commun* 2019;**10**:4871.
29. Ma YC, Zhang YX, Li XQ, Zhao YY, Li M, Jiang W, et al. Near-infrared II phototherapy induces deep tissue immunogenic cell death and potentiates cancer immunotherapy. *ACS Nano* 2019;**13**:11967−80.
30. Sweeney EE, Cano-Mejia J, Fernandes R. Photothermal therapy generates a thermal window of immunogenic cell death in neuroblastoma. *Small* 2018;**14**:1800678.
31. Zhou ZW, Wu H, Yang RX, Xu A, Zhang QY, Dong JW, et al. GSH depletion liposome adjuvant for augmenting the photothermal immunotherapy of breast cancer. *Sci Adv* 2020;**6**:4373.
32. Xu Z, Huang HB, Xiong X, Wei XQ, Guo X, Zhao JY, et al. A near-infrared light-responsive extracellular vesicle as a "Trojan horse" for tumor deep penetration and imaging-guided therapy. *Biomaterials* 2021;**269**:120647.
33. Xiong X, Xu Z, Huang HB, Wang Y, Zhao JY, Guo X, et al. A NIR light triggered disintegratable nanoplatform for enhanced penetration and chemotherapy in deep tumor tissues. *Biomaterials* 2020;**245**:119840.
34. Liu R, Hu C, Yang YY, Zhang JQ, Gao HL. Theranostic nanoparticles with tumor-specific enzyme-triggered size reduction and drug release to perform photothermal therapy for breast cancer treatment. *Acta Pharm Sin B* 2019;**9**:410−20.
35. Yang Y, Zhu WJ, Dong ZL, Chao Y, Xu L, Chen MW, et al. 1D coordination polymer nanofibers for low-temperature photothermal therapy. *Adv Mater* 2017;**29**:1703588.
36. Sun T, Zhang GP, Wang QB, Chen QJ, Chen XL, Lu YF, et al. A targeting theranostics nanomedicine as an alternative approach for hyperthermia perfusion. *Biomaterials* 2018;**183**:268−79.
37. Li XM, Zhang YH, Ma ZQ, He CJ, Wu YL, An Q, et al. Designing cancer nanodrugs that are highly loaded, pH-responsive, photothermal, and possess a favored morphology: a hierarchical assembly of DOX and layer-by-layer modified rGO. *Chin Chem Lett* 2019;**30**:489−93.
38. Zhao JY, Zhong D, Zhou SB. NIR-I-to-NIR-II fluorescent nanomaterials for biomedical imaging and cancer therapy. *J Mater Chem B* 2018;**6**:349−65.
39. Yang T, Tang YA, Liu L, Lv XY, Wang QL, Ke HT, et al. Size-dependent Ag_2S nanodots for second near-infrared fluorescence/photoacoustics imaging and simultaneous photothermal therapy. *ACS Nano* 2017;**11**:1848−57.
40. Aydemir D, Hashemkhani M, Durmusoglu EG, Acar HY, Ulusu NN. A new substrate for glutathione reductase: glutathione coated Ag_2S quantum dots. *Talanta* 2019;**194**:501−6.
41. Hu QL, Wu M, Fang C, Cheng CY, Zhao MM, Fang WH, et al. Engineering nanoparticle-coated bacteria as oral DNA vaccines for cancer immunotherapy. *Nano Lett* 2015;**15**:2732−9.
42. Tang H, Xu X, Chen Y, Xin H, Wan T, Li B, et al. Reprogramming the tumor microenvironment through second-near-infrared-window photothermal genome editing of PD-L1 mediated by supramolecular gold nanorods for enhanced cancer immunotherapy. *Adv Mater* 2021;**33**:2006003.
43. Wei X, Liu LQ, Li XL, Wang Y, Guo X, Zhao JY, et al. Selectively targeting tumor-associated macrophages and tumor cells with polymeric micelles for enhanced cancer chemo-immunotherapy. *J Control Release* 2019;**313**:42−53.
44. He LZ, Nie TQ, Xia XJ, Liu T, Huang YY, Wang XJ, et al. Designing bioinspired 2D $MoSe_2$ nanosheet for efficient photothermal-triggered cancer immunotherapy with reprogramming tumor-associated macrophages. *Adv Funct Mater* 2019;**29**:1901240.